Modelling the viscoelastic mechanosorptive behaviour of Norway spruce under long-term compression perpendicular to the grain

Francesco Mirko Massaro [1*], *Kjell Arne Malo* [1]

[1] Department of Structural Engineering, Norwegian University of Science and Technology (NTNU), Rich. Birkelandsvei 1A, 7491, Trondheim, Norway

[*] corresponding author, francesco.m.massaro@ntnu.no

ABSTRACT

The effects of variation in humidity coupled with long-term loading give rise to dimensional changes and the creep effects in wooden elements. Many wooden products such as cross-laminated timber (CLT) plates as well as many common structural details used in timber engineering are vulnerable to variations in moisture content (MC) as well as to creep effects. This paper addresses the long-term effects in the material modelling of timber by the finite element method (FEM), also considering the viscoelastic and mechanosorptive effects in wood. The model was calibrated using both relaxation tests and creep tests. The results from both long-term compression perpendicular-to-grain tests (relaxation and creep) performed on glulam (GL30c) from Norway spruce (*Picea abies*) with moisture control are presented in the paper. The material model considers the effect of loading and moisture changes. For realistic comparison, the pith location of each lamella was specified in the numerical analyses. Ultimately, a comparison between the numerical results and the experimental results has been provided, exhibiting an overall good estimation of timber response.

Keywords

creep, long-term behaviour, mechanosorptive, compression perpendicular to grain, timber properties

1. INTRODUCTION

Traditional timber structures mostly utilise one-dimensional (1D) members as beams and columns. However, with the introduction of large cross-laminated timber (CLT) elements in medium-rise timber buildings, a transition to the use of more two-dimensional (2D) elements has taken place. A similar development is experienced in modern timber bridge buildings, but in this case the deck is most commonly made of stress-laminated plates (SLPs), i.e. parallel beams transversely pre-tensioned together by tension rods. SLPs have become very popular as deck elements for larger timber bridges. Both types of timber plates are, to some degree, vulnerable to long-term properties of the wooden material used to produce the plates. The dimensional change due to moisture and the significant creep effect might lead to warping of CLT plates and loss of pretension in SLPs. In the production of CLT plates, this potential problem is minimised by restricting the lay-up to symmetric and orthotropic stacks of lamellas. For SLPs, the problem is handled using very high-strength pretension cables along with restressing procedures during the structure's lifetime.

However, it is possible to address the long-term effects through improvements in the material modelling of timber, also considering the viscoelastic and mechanosorptive effects in wood. Therefore, the finite element method (FEM) models for the optimisation of timber plates have become more available, and improved timber products might be developed. This study focused on the long-term effect of compression perpendicular to the grain as it represents a loading situation which characterises several common timber structures and structural layouts such as stress-laminated timber decks, wooden elements lying in between vertical load-bearing supports as well as traditional timber-to-timber joints. Moreover, understanding the dependency on time and moisture changes in the behaviour of structural timber, when loaded, is a key subject in timber engineering.

The primary objective of this research was to accurately model timber subjected to compression perpendicular to the grain. The modelling procedure considers the effects of time and moisture variations on the basis of the model described by Fortino et al. (2009), also conferring Toratti (1992) and Hanhijärvi and Mackenzie-Helnwein (2003). The additional deformation due to concurrent loading and moisture content (MC) changes below the fibre saturation point is known as the mechanosorptive effect (Hunt 1994). As shown by Muszyński et al. (2005), it is necessary to know the MC distribution in the timber elements to properly evaluate the mechanosorptive effect. Therefore, the stress-strain analysis is coupled with a moisture diffusion analysis. The use of Kelvin-type models to describe the mechanosorptive deformation has been suggested by several authors (Hanhijärvi 1995, Salin 1992, Toratti 1992). In Lagaňa et al. (2011), a Kelvin body is connected in series with a Newtonian dashpot in order to obtain different mechanosorptive behaviours in tension and in compression. In this study, the approach developed by Svensson and Toratti (2002) was used. Ozyhar et al. (2013) performed tests to study the viscoelastic behaviour of timber, including timber under compression perpendicular to the grain for 24 h.

This paper deals with two independent experimental test procedures. In one procedure, the load on the specimens was constant, resulting in a creep test whereas in the second, the strain was maintained constant and therefore data on the relaxation of timber were obtained. In both the experiments, the timber specimens were compressed perpendicular to the grain and exposed to changes in the MC caused by variations in the relative humidity (RH) of the surrounding air. The material parameters were determined based on the results of the creep test and then validated utilising the results of the relaxation test. The numerical model was implemented in the software Abaqus (Dassault Systemes 2014) by means of user subroutines.

2. MATERIAL AND METHODS

2.1 CONSTITUTIVE MODEL

The material model used for the analysis was developed by Fortino et al. (2009) and expresses the total strain rate $\dot{\boldsymbol{\varepsilon}}$ as the sum of the elastic strain rate $\dot{\boldsymbol{\varepsilon}}_e$, the shrinkage-swelling strain rate $\dot{\boldsymbol{\varepsilon}}_s$, the viscoelastic strain rate $\dot{\boldsymbol{\varepsilon}}_v$ and the mechanosorptive strain rate $\dot{\boldsymbol{\varepsilon}}_{ms}$ as shown in Equation (1).

$$\dot{\boldsymbol{\varepsilon}} = \dot{\boldsymbol{\varepsilon}}_e + \dot{\boldsymbol{\varepsilon}}_s + \dot{\boldsymbol{\varepsilon}}_v + \dot{\boldsymbol{\varepsilon}}_{ms} \tag{1}$$

Elastic deformation

The elastic strain $\boldsymbol{\varepsilon}_e$ is provided by the Hooke's law, Equation (2), where $\boldsymbol{C}_e$ is the elastic stiffness and $\boldsymbol{\sigma}$ represents the stress.

$$\boldsymbol{\sigma} = \boldsymbol{C}_e\, \boldsymbol{\varepsilon}_e \tag{2}$$

The rate form of the inverse Hooke's law is given in Equation (3), and it takes into account the variation of timber stiffness due to MC variations.

$$\dot{\boldsymbol{\varepsilon}}_e = \dot{\boldsymbol{S}}_e\boldsymbol{\sigma} + \boldsymbol{S}_e\dot{\boldsymbol{\sigma}} \tag{3}$$

As timber is reasonably described as an orthotropic material, there exist only nine non-zero independent stiffness terms and therefore the elastic compliance $\boldsymbol{S}_e$ can be expressed as shown in (4).

$$\boldsymbol{S}_e = \boldsymbol{C}_e^{-1} = \begin{bmatrix} 1/E_R & -\nu_{TR}/E_T & -\nu_{LR}/E_L & 0 & 0 & 0 \\ -\nu_{RT}/E_R & 1/E_T & -\nu_{LT}/E_L & 0 & 0 & 0 \\ -\nu_{RL}/E_R & -\nu_{TL}/E_T & 1/E_L & 0 & 0 & 0 \\ 0 & 0 & 0 & 1/G_{RT} & 0 & 0 \\ 0 & 0 & 0 & 0 & 1/G_{RL} & 0 \\ 0 & 0 & 0 & 0 & 0 & 1/G_{TL} \end{bmatrix} \quad (4)$$

The dependence on the MC variations of both the moduli of elasticity E_i and the shear moduli G_{ij} can be approximated as in Equation (5) according to Santaoja et al. (1991). Here, $S_{e_{ij}}$ represents a component of the compliance $\boldsymbol{S}_e$, and the reference values correspond to an MC of 12%.

$$S_{e_{ij}} = \frac{S_{e_{ij,ref}}}{[1 - 2.6(u - u_{ref})]} \qquad u_{ref} = 0.12 \quad (5)$$

The longitudinal stiffness modulus E_L was selected as the mean longitudinal stiffness of the inner layers of GL30c according to EN338:2016 (CEN 2016), while the other properties were obtained from the studies by Dahl (Dahl 2009, Dahl and Malo 2009). The reference values of the elastic properties are given in Table 1.

Table 1: Reference elastic properties. E_L: (CEN 2016); all other properties: (Dahl 2009, Dahl and Malo 2009).

Normal modulus	(MPa)	Shear modulus	(MPa)	Poisson's ratio	(-)
E_R	818	$G_{RT} = G_{TR}$	31	ν_{RT}	0.835
E_T	352	$G_{LR} = G_{RL}$	641	ν_{LR}	0.501
E_L	11500	$G_{LT} = G_{TL}$	582	ν_{LT}	0.695

Hygroscopic deformation

The hygroscopic strain rate $\dot{\boldsymbol{\varepsilon}}_s$ is directly dependent on the rate of MC $\dot{u}$ as shown in Equation (6) through the hygro-expansion vector $\boldsymbol{\alpha}$.

$$\dot{\boldsymbol{\varepsilon}}_s = \boldsymbol{\alpha}\,\dot{u} \tag{6}$$

$$\boldsymbol{\alpha} = [\alpha_R, \alpha_T, \alpha_L, 0\ , 0\ , 0]^T \tag{7}$$

In (7), α_R, α_T and α_L are the hygro-expansion coefficients for the radial, tangential and longitudinal directions relative to grain direction, respectively.

The wetting and drying processes involve different mechanisms, and this leads to a difference in the dimensional changes between the two phases. Indeed, it has been demonstrated that the hygro-expansion coefficients in the direction perpendicular to the grain have different values in the two processes (Angst and Malo 2012). The values used herein are calibrated based on the described creep experiment. Regarding the dimensional changes in the longitudinal direction, the coefficient proposed by Fortino et al. (2009) was selected for both phases, as these changes have a different order of magnitude. The complete set of coefficients used in the model also agrees well with Dinwoodie (2000) and is presented in Table 2.

Table 2: Hygro-expansion coefficients, α_L:(Fortino et al. 2009).

	α_T	α_R	α_L
wetting	0.154	0.085	0.005
drying	0.134	0.074	0.005

Viscoelastic deformation

The viscoelastic strain $\boldsymbol{\varepsilon}_v$ is a component of the total deformation dependent on time. According to Hanhijärvi and Mackenzie-Helnwein (2003), the development of this component of the strain can be described by a Kelvin viscoelastic body realised as an elastic spring and a viscous dashpot connected in parallel.

The behaviour of a Kelvin body can be described by Equation (8) in which the first term in the summation refers to the stress in the spring, and the second term refers to the dashpot (Zienkiewicz et al. 1968).

$$\boldsymbol{\sigma} = \boldsymbol{C}_v \boldsymbol{\varepsilon}_v + \tau\, \boldsymbol{C}_v \dot{\boldsymbol{\varepsilon}}_v \tag{8}$$

In Equation (8), τ is the retardation time of the dashpot and $\boldsymbol{C}_v$ is the stiffness of the Kelvin body. Introducing $\boldsymbol{C}_v^{-1} = J_i(\sigma)\boldsymbol{C}_e^{-1}$, Equation (8) can be rearranged as in the differential equation (9) in which the subscript i refers to the i^{th} element in a series of Kelvin bodies and $J_i(\sigma)$ is a dimensionless scalar.

$$\dot{\boldsymbol{\varepsilon}}_{v,i} + \frac{1}{\tau_i}\boldsymbol{\varepsilon}_{v,i} = \frac{1}{\tau_i} J_i(\sigma)\boldsymbol{C}_e^{-1} : \boldsymbol{\sigma} \tag{9}$$

It has been reported that the hypothesis of linear viscoelastic behaviour of timber is valid only under a certain stress level (Dinwoodie 2000, Schniewind 1968, Toratti 1992). Moreover, the threshold stress for linear viscoelastic behaviour is around 30%–40% of the characteristic short-term strength (Morlier and Palka 1994). In this study, the linear viscoelastic behaviour is maintained until the compression stress perpendicular to the grain exceeds 0.8 MPa. Above this stress level, the behaviour of timber is non-linear, and the dependency of J_i on stress is as described in Equation (10).

$$\begin{cases} J_i = J_{0,i}, & \sigma_\perp < 0.8\ MPa \\ J_i = J_{0,i}\left(\dfrac{\sigma_\perp}{\sigma_{ref}}\right)^k, & \sigma_\perp \geq 0.8\ MPa \end{cases} \tag{10}$$

In Equation (10), $J_{0,i}$ is the value of J_i when timber behaves as a linear viscoelastic material, the reference stress σ_{ref} is equal to 0.8 MPa, and $\sigma_\perp$ is the transverse to grain compressive stress. The values of $J_{0,i}$ and τ_i used in this material model are given in Table 3, considering the total viscoelastic deformation as distributed in six viscoelastic Kelvin bodies. The scalar exponent k is chosen equal to 0.879. The values of these parameters are selected in order to fit the first phase with constant RH of the air of the creep experiment results.

Table 3: Linear viscoelastic compliances of the element i relative to the elastic compliances, $J_{0,i}$, and their retardation time τ_i.

τ_i (days)	$J_{0,i}$ (-)
0.1	0.459
1	0.087
10	0.129
100	0.317
1000	0.383
10000	0.451

Mechanosorptive deformation

The mechanosorptive deformation is the component of deformation due to the interaction of stress and moisture content variations.

Svensson and Toratti (2002) demonstrated that the mechanosorptive strain $\boldsymbol{\varepsilon}_{ms}$ can be expressed as the sum of the recoverable part of the mechanosorptive strain, $\boldsymbol{\varepsilon}_{ms,r}$, and the irrecoverable part of the mechanosorptive strain, $\boldsymbol{\varepsilon}_{ms,ir}$, as expressed by Equation (11).

$$\boldsymbol{\varepsilon}_{ms} = \boldsymbol{\varepsilon}_{ms,r} + \boldsymbol{\varepsilon}_{ms,ir} \tag{11}$$

Furthermore, the evolution of the recoverable mechanosorptive strain for each mechanosorptive Kelvin body j is similar to the viscoelastic one; see Equation (9). In Equation (12) for the element j, $\boldsymbol{S}_{\infty,j}$ is the compliance at the mechanosorptive creep limit defined by Equation (14), τ_j is a dimensionless material parameter (Fortino et al. 2009, Hanhijärvi and Mackenzie-Helnwein 2003) and $\dot{u}$ is the moisture content change rate.

$$\dot{\boldsymbol{\varepsilon}}_{ms,r,j} + \frac{|\dot{u}|}{\tau_j}\boldsymbol{\varepsilon}_{ms,r,j} = \frac{|\dot{u}|}{\tau_j}\boldsymbol{S}_{\infty,j}\colon\boldsymbol{\sigma} \tag{12}$$

The irrecoverable mechanosorptive strain exists only in the presence of moisture content never reached before by the loaded timber element (Svensson and Toratti 2002).

$$\dot{\boldsymbol{\varepsilon}}_{ms,ir} = \boldsymbol{S}_{mi}\boldsymbol{\sigma}\left|\dot{U}\right| \tag{13}$$

In Equation (13), $\dot{U}$ is a moisture content rate for a value not previously reached in the load history of the material. The irrecoverable mechanosorptive compliance $\boldsymbol{S}_{mi}$ is defined as shown in Equation (15) (Fortino et al. 2009).

$$\boldsymbol{S}_{\infty} = \begin{bmatrix} \frac{m_T E_T}{E_R} & -\nu_{TR} m_T & -\frac{\nu_{LR} m_T E_T}{E_L} & 0 & 0 & 0 \\ -\frac{\nu_{RT} m_T E_T}{E_R} & m_T & -\frac{\nu_{LT} m_T E_T}{E_L} & 0 & 0 & 0 \\ -\frac{\nu_{RL} m_T E_T}{E_R} & -\nu_{TL} m_T & m_L & 0 & 0 & 0 \\ 0 & 0 & 0 & \frac{m_T E_T}{G_{RT}} & 0 & 0 \\ 0 & 0 & 0 & 0 & \frac{m_T E_T}{G_{RL}} & 0 \\ 0 & 0 & 0 & 0 & 0 & \frac{m_T E_T}{G_{TL}} \end{bmatrix} \tag{14}$$

$$\boldsymbol{S}_{mi} = \begin{bmatrix} \frac{m_{vT} E_T}{E_R} & -\nu_{TR} m_{vT} & 0 & 0 & 0 & 0 \\ -\frac{\nu_{RT} m_{vT} E_T}{E_R} & m_{vT} & 0 & 0 & 0 & 0 \\ 0 & 0 & 0 & 0 & 0 & 0 \\ 0 & 0 & 0 & \frac{m_{vT} E_T}{G_{RT}} & 0 & 0 \\ 0 & 0 & 0 & 0 & \frac{m_{vT} E_T}{G_{RL}} & 0 \\ 0 & 0 & 0 & 0 & 0 & \frac{m_{vT} E_T}{G_{TL}} \end{bmatrix} \tag{15}$$

In Equation (14), m_T and m_L are the limit mechanosorptive compliances in the tangential and longitudinal direction, respectively, and in Equation (15), m_{vT} is the irrecoverable mechanosorptive tangential parameter equal to 0.0298 MPa^{-1} with the parameter in the longitudinal direction set to zero. The recoverable mechanosorptive strain is allotted among three mechanosorptive Kelvin bodies with the parameters given in Table 4.

The longitudinal mechanosorptive limit compliance values m_L were introduced by Toratti (1992) and allotted among the three Kelvin bodies according to Fortino et al. (2009). The tangential mechanosorptive limit compliance m_T and the tangential irrecoverable mechanosorptive parameter m_{vT} were calibrated based on the measured results of the creep experiment.

Table 4: Parameters used in the recoverable mechanosorptive constitutive equation. m_L: (Fortino et al. 2009, Toratti 1992).

j	τ_j (-)	m_T (MPa^{-1})	m_L (MPa^{-1})
1	0.01	0.0016	0.175/E_L
2	0.1	0.0016	0.490/E_L
3	1	0.0160	0.035/E_L

2.2 MOISTURE TRANSPORT MODEL

It is assumed that the moisture transport in the timber follows Fick's second law of diffusion shown in Equation (16).

$$\frac{\partial u}{\partial t} = \nabla \cdot (\boldsymbol{D}\, \nabla u) \tag{16}$$

The diffusivity $\boldsymbol{D}$ depends on the moisture content level u. In the present analyses, the expression provided by Fortino et al. (2009), as given in Equation (17), is used for the diffusion coefficients in transverse directions D_R and D_T.

$$D_R = D_T = 2.4 \cdot 10^{-4} e^{4u} \quad \mathrm{mm^2 s^{-1}} \tag{17}$$

The values obtained by Sjödin (2006) for Norway Spruce (*Picea abies*) are used for the diffusion coefficient in longitudinal direction D_L. The diffusion coefficients are plotted in Figure 1 showing their dependency on the moisture content MC.

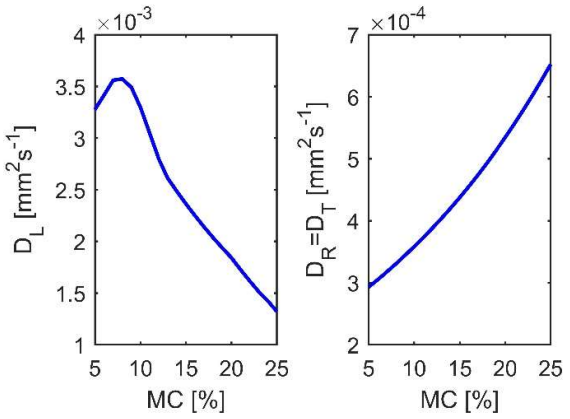

Figure 1: Diffusion coefficients in the longitudinal direction and in the transverse direction of Norway spruce.

The moisture diffusion Equation (16) is similar to the heat transfer Equation (18) where ρ is the density of timber, c_T is the specific heat, T is temperature and $\boldsymbol{\lambda}$ is the thermal conductivity. By letting $\boldsymbol{\lambda} = \rho \boldsymbol{D}$ and $c_T = 1$, the heat transfer formulation can also be used for moisture diffusion, Equation (16).

$$\rho c_T \frac{\partial T}{\partial t} = \nabla \cdot (\boldsymbol{\lambda} \nabla T) \tag{18}$$

Due to this analogy described by Fortino et al. (2009), the moisture diffusion analyses were conducted as thermal diffusion analyses implemented in the user subroutine DFLUX of the software Abaqus in which the RH of the air is given as the input and both the moisture flux and its rate of change are obtained as the output.

The moisture flux across the boundary is driven by the difference between the MC at the surface of timber u_{surf} and the equilibrium MC of timber for the current RH of the air u_{eq}.

$$(\boldsymbol{D} \nabla u) = S(u_{eq} - u_{surf}) \tag{19}$$

In Equation (19), the surface emission factor S is considered equal to $10 \cdot 10^{-8}\ m \cdot s^{-1}$ (Angst and Malo 2013).

The equilibrium MC u_{eq} is calculated by Equation (20) in accordance with Avramidis (1989) such that the temperature T is expressed in Kelvin and RH is the relative humidity of the air.

$$u_{eq} = 0.01 \left[\frac{-T \ln(1 - RH)}{0.13 \left(1 - \frac{T}{647.1}\right)^{-6.46}} \right]^{\frac{1}{110T^{-0.75}}} \tag{20}$$

2.3 NUMERICAL MODEL

Elastic and hygroscopic strain increment

The elastic strain increment $\Delta\boldsymbol{\varepsilon}_e$ expressed in Equation (21) is obtained from Equation (3).

$$\Delta\boldsymbol{\varepsilon}_e = \Delta\boldsymbol{S}_e\boldsymbol{\sigma} + \boldsymbol{S}_e\Delta\boldsymbol{\sigma} \tag{21}$$

The variation of the elastic compliance $\Delta\boldsymbol{S}_e$ is due to the variation in the MC described by Equation (5).

The hygroscopic strain increment $\Delta\boldsymbol{\varepsilon}_s$, Equation (22), is straightforwardly obtained from Equation (6).

$$\Delta\boldsymbol{\varepsilon}_s = \boldsymbol{\alpha}\Delta u \tag{22}$$

Viscoelastic strain increment

The viscoelastic strain increment $\Delta\boldsymbol{\varepsilon}_v$ for each Kelvin body is obtained by solving Equation (9).

$$\begin{aligned}\Delta\boldsymbol{\varepsilon}_v = \boldsymbol{\varepsilon}_{v,n}\left(e^{-\xi} - 1\right) + \left[\boldsymbol{C}_e^{-1}J_{n+1}\left(T_{n+1} + T_{n,n+1}\right) + \boldsymbol{C}_e^{-1}J_n\left(T_n + T_{n+1,n}\right)\right]\boldsymbol{\sigma}_n \\ + \left(\boldsymbol{C}_e^{-1}J_{n+1}T_{n+1} + \boldsymbol{C}_e^{-1}J_nT_{n+1,n}\right)\Delta\boldsymbol{\sigma}\end{aligned} \tag{23}$$

In Equation (23), n denotes the increment number, $\boldsymbol{\sigma}$ is the stress, $\boldsymbol{\varepsilon}_v$ is the creep strain, $\boldsymbol{C}_e$ is the elastic stiffness, J represents the ratio between the final compliance of the viscoelastic Kelvin body and the elastic compliance. Furthermore, T is function of the pseudo-time parameter $\xi = \Delta t/\tau$, with T_n, $T_{n,n+1}$ and T_{n+1} specified in Equation (24)

$$T_n = -e^{-\xi} - \frac{2e^{-\xi}}{\xi} + \frac{2}{\xi^2} - \frac{2e^{-\xi}}{\xi^2}$$

$$T_{n,n+1} = \frac{1}{\xi} - \frac{e^{-\xi}}{\xi} - \frac{2}{\xi^2} + \frac{2}{\xi^2}e^{-\xi} \tag{24}$$

$$T_{n+1} = 1 - \frac{2}{\xi} + \frac{2}{\xi^2} - \frac{2}{\xi^2}e^{-\xi}$$

A detailed derivation of Equation (23) is given in the Appendix.

Mechanosorptive strain increment

The mechanosorptive recoverable strain increment $\Delta\boldsymbol{\varepsilon}_{ms,r}$, given by Equation (25), is evaluated similar to the creep strain increment.

$$\Delta\boldsymbol{\varepsilon}_{ms,r} = \boldsymbol{\varepsilon}_{ms,r,n}(e^{-\chi} - 1) + \boldsymbol{S}_{\infty}\boldsymbol{\sigma}_n(\mathcal{T}_{n+1} + \mathcal{T}_n) + \boldsymbol{S}_{\infty}\Delta\boldsymbol{\sigma}\mathcal{T}_{n+1} \tag{25}$$

Here, $\mathcal{T}$ is function of the parameter $\chi = \Delta u/\tau$, with $\mathcal{T}_n$ and $\mathcal{T}_{n+1}$ given in Equation (26).

$$\mathcal{T}_n = 1/\chi - e^{-\chi} - e^{-\chi}/\chi$$

$$\mathcal{T}_{n+1} = 1 - \frac{1}{\chi} + e^{-\chi}/\chi \tag{26}$$

A detailed derivation of Equation (25) is given in the Appendix.

The mechanosorptive irrecoverable strain $\Delta\boldsymbol{\varepsilon}_{ms,i}$ is obtained directly from Equation (13) and thus computed by Equation (27).

$$\Delta\boldsymbol{\varepsilon}_{ms,i} = \boldsymbol{S}_{mi}\boldsymbol{\sigma}|\Delta U| \tag{27}$$

Implementation of the algorithm

The stress update algorithm is implemented in the user subroutine UMAT of the software Abaqus. At the beginning of a new time step t_{n+1}, the MC u_{n+1} and its increment $\Delta u = u_{n+1} - u_n$ are evaluated by the user subroutine DFLUX, and the total strain increment $\Delta\boldsymbol{\varepsilon}$ is given by the variable DSTRAN. Moreover, it is assumed that the total stress increment $\Delta\boldsymbol{\sigma}$, the elemental

viscoelastic strain increment $\Delta\boldsymbol{\varepsilon}_{v,i}$ and the elemental mechanosorptive increment $\Delta\boldsymbol{\varepsilon}_{ms,r,j}$ are equal to zero. The elastic compliance and the mechanosorptive irrecoverable compliance matrix are computed and therefore, it is possible to compute the trial stress and update the viscoelastic parameter $J_{n+1}^{(k)}$. Here, the superscript *k* indicates the iterations within the same time increment. Thereafter, the tangent stiffness operator is computed. The stress update is computed, updating the elemental viscoelastic strain and the elemental mechanosorptive strain. Furthermore, the residual vectors from Equations (21), (23) and (25) are calculated and if the norm is greater than a selected tolerance, a new iteration is performed computing a new trial stress. If convergence is reached, the final values of the strains are stored and the algorithm moves on to the next time step.

2.4 EXPERIMENTAL TESTS

Long-term compression tests were conducted on Norway Spruce specimens classified as GL30c according to NS-EN 14080:2013 (CEN 2013) and manufactured by Moelven Limtre AS (Moelv, Norway). Two different types of tests were performed: relaxation tests and creep tests. In the relaxation tests, the deformation of timber was kept constant during the experiment, while in the creep tests, the load applied to the timber specimen was constant for the entire duration of the tests.

Glulam of class GL30c was selected for testing due to the common use of this type of beams in timber decks for bridges. Stress-laminated deck plates usually have their pre-tensioning cables located in their softer inner lamellas. Moreover, in CLT lay-ups transmitting high transversal loads, the softer layers will probably dominate the response. Therefore, the specimens were conservatively obtained by cutting a timber beam with cross-section 360×140 mm^2 in order to utilise only the softer inner lamellas as the outer lamellas have different properties than the

inner ones (GL30c). Therefore, the four external lamellas were removed obtaining specimens made only by the four softer inner lamellas.

2.4.1 RELAXATION TESTS

For the preparation of the specimens for the relaxation tests, the inner lamellas were sliced along the longitudinal direction every 230 mm, thereby obtaining cuboids of dimension 140×230×180 mm^3 (Figure 2).

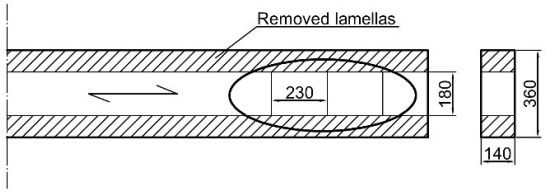

Figure 2: Location of the cuboidal specimen in a glulam beam (dimensions in mm).

Two specimens were made each of two cuboids of dimension 140×230×180 mm^3. Both specimens had a 33-mm diameter hole in the centre of the loaded faces to allow the insertion of a 30-mm diameter steel threaded rod. The total height of the specimens was 360 mm (Figure 3).

The specimens were placed in between two steel plates of dimension 330×200×20 mm^3 to achieve a proper distribution of the compression load induced by a pre-stressed rod. Both plates comprise a hole in the centre to allow the rod's passage.

A threaded rod of 30 mm diameter was inserted into the hole holding the cuboids together. The rod was inserted perpendicular to the direction of the wood fibres and then tightened, thereby compressing the specimens in the perpendicular direction (Figure 3).

The rod was pre-stressed using a hydraulic machine. The load was measured and monitored for the whole duration of the experiment using a ring load cell located between the bottom steel plate and the fastening nut.

In addition, two transducers [linear variable displacement transducers (LVDTs)] were placed on the end faces of the specimens, also covering the interface between the cuboids, in order to verify that the strain in the specimens remained approximately constant during the tests (Figure 3).

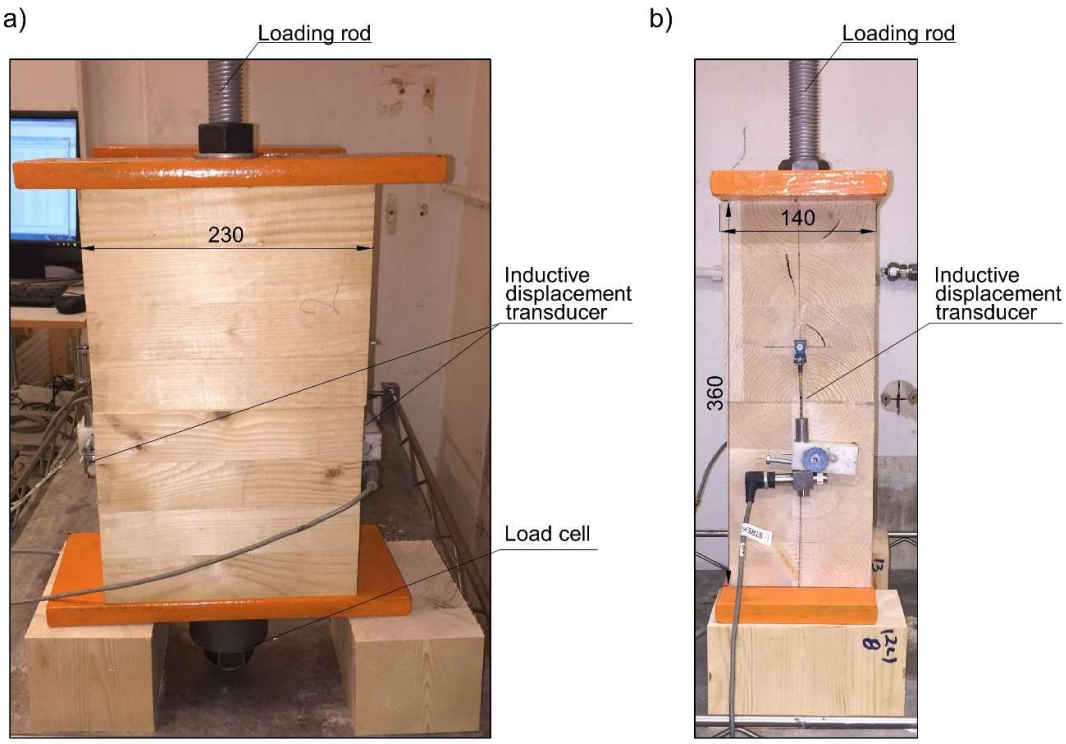

Figure 3: Pictures of the test setup (dimensions in mm). a) Location of measuring transducers (LVDT) and load cell; b) Location of LVDT.

The tests were initially performed in a climate-controlled room with a constant temperature of 20°C and continuous controlled RH of the air. In this initial phase which lasted almost 2 months, the two specimens were tested under a constant RH of 65%. Therefore, it was possible to evaluate the relaxation of the stresses in the specimens due to viscoelastic effects without the influence of the MC variations in the wood. Afterwards, the specimens were placed in a sealed climate-controlled chamber (see Figure 4) to vary the RH between 80% and 40% with the aim of evaluating the mechanosorptive effects on the specimens. The variation of RH vs. time of the surrounding air is depicted in Figure 6.

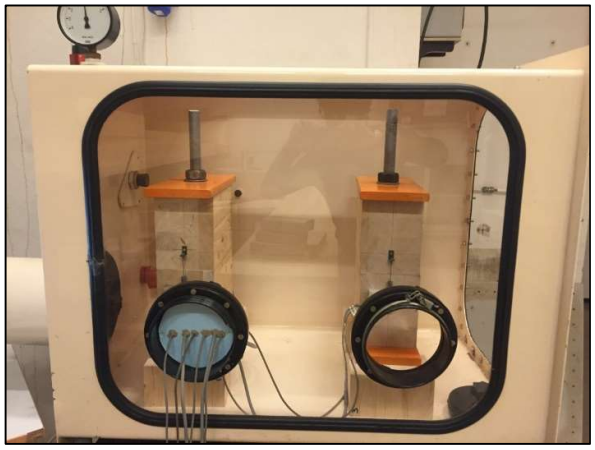

Figure 4: Specimens and setup into the sealed climate-controlled chamber.

The variations in RH during the experimental relaxation tests were controlled with the use of saturated salt solutions inserted in the chamber. The two saturated salt solutions were ammonium sulphate [$(NH_4)_2SO_4$] to provide an 80% RH and potassium carbonate (K_2CO_3) to reach a 50% RH. A technical issue of the climate room brought the RH further down to around 40% as shown in Figure 6. However, the presence of two moisture loggers allowed for proper evaluation of the RH of the air surrounding the specimens.

The two specimen setups were tested under two different load conditions corresponding to the perpendicular-to-grain compression stresses on the timber of 0.8 and 1 MPa, respectively. The compression stress values were chosen in order to reproduce the stress levels of interest in real structures and to match the load conditions in the accompanying creep test setups.

2.4.2 CREEP TESTS

Long-term compression tests were performed with a constant level of stress. The tests were performed on nine timber specimens of Norway spruce (GL30c). The specimens were cut out of the inner lamellas in a manner similar to the relaxation tests (see Figure 2) and assembled by stacking five cuboids of dimension 100×115×180 mm^3, resulting in a total height of 900 mm.

The specimens had holes of 22 mm diameter in the centre of the cuboids' minor faces to insert tension rods of 16 mm diameter. The tension rods were running through the holes and were connected to steel plates at the top of the stacks which in turn distributed the loads and imposed compression perpendicular to grain on the specimens (Figure 5).

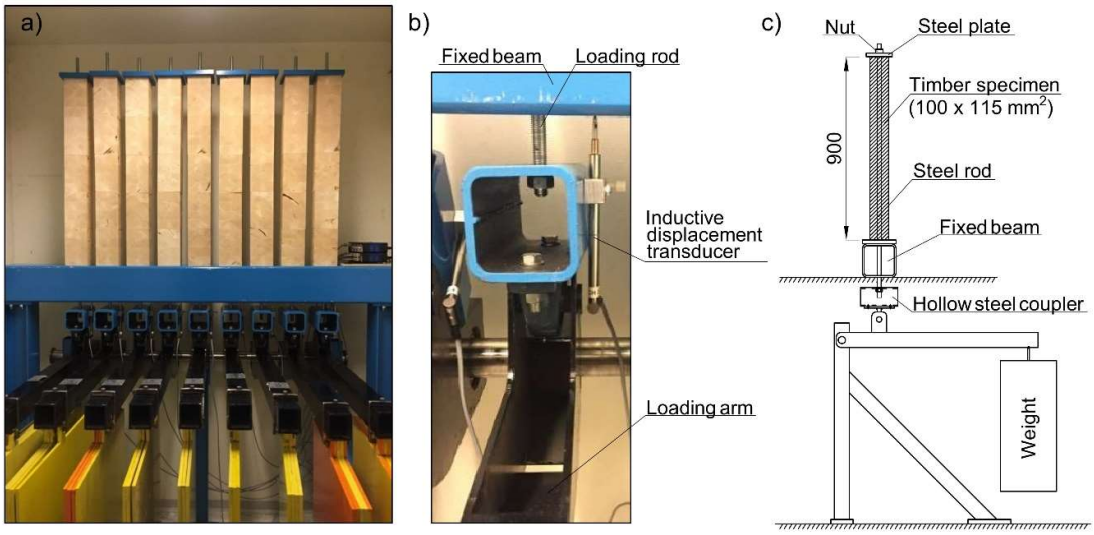

Figure 5: Pictures of the creep experimental setup. a) Detail of the experimental setup showing the timber specimens loaded with a different number of steel plates (yellow) through lever arms (black); b) Detail of a measuring transducer showing the hollow steel coupler between the loading rod and the lever arm; c) Sketch of the setup (dimensions in mm).

The tests were performed in a climate-controlled room with a constant temperature of 20°C. The RH of the chamber varied between 50% and 80% during the test as shown in Figure 7. The specimens were loaded with three different uniform values of perpendicular compression stress of 0.6, 0.8 and 1 MPa using lever arms loaded with different dead weights at the tip (see Figure 5a). The long-term deformations were monitored by inductive displacement transducers (Figure 5b) which, after subtracting the elastic elongation of the rods, provided the vertical dimensional change of the wooden specimens solely.

3. RESULTS AND DISCUSSION

3.1 EXPERIMENTAL RESULTS

3.1.1 RELAXATION TEST RESULTS

Constant climate conditions

For a period of almost 3 months, the specimens were tested keeping the temperature and the RH of the surrounding air constant, respectively, at 20°C and 65%.

Moreover, the deformation of timber was kept constant and therefore the stress was expected to decrease over time due to the viscoelastic behaviour of timber (see Figure 6).

Indeed, a decrease was observed in the pre-stressing force of the rods and consequently, perpendicular compression stresses on the specimens also appeared reduced.

Variable relative humidity

In the second phase of the test procedure, the experimental setup was moved into a sealed climate-controlled chamber (Figure 4) and subjected to changes in the RH of the air surrounding the timber specimens depicted in Figure 6. However, a technical issue in the chamber led to a RH of 40%; see Figure 6. Nevertheless, as the temperature and the RH in the chamber were constantly monitored using four loggers, two of which registered temperature data and two recorded moisture data, the experimental procedure was changed but not affected otherwise.

The drying and consequently the change of dimension led to almost zero stress in the specimens. The measured deformations between the two timber blocks (Figure 3b) remained fairly constant throughout the test. A minor change in the deformation was observed at the onset of drying but it returned to the original value at the beginning of the subsequent wetting phase.

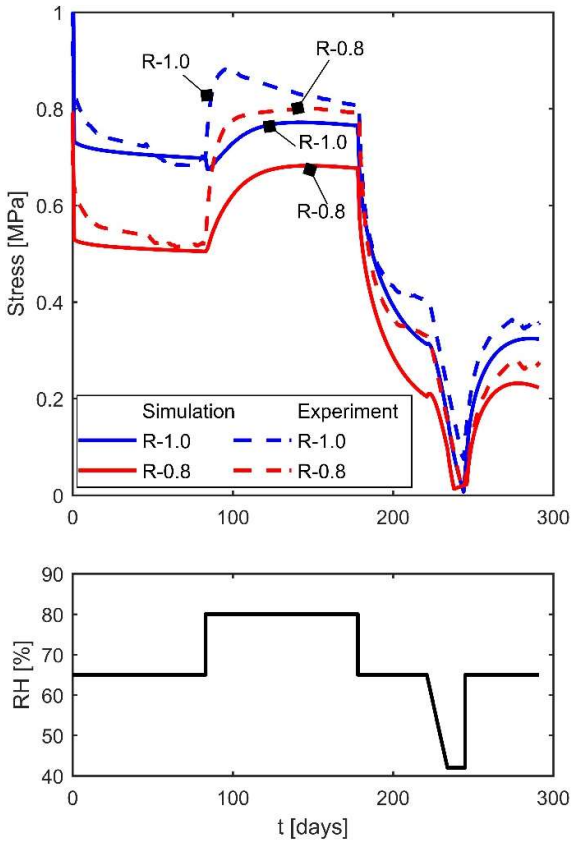

Figure 6: Comparison between numerical and experimental results of the relaxation tests and relative humidity (RH) of the air during the relaxation tests (Norway spruce).

3.2 DISCUSSION OF THE NUMERICAL RESULTS

The experimental setups described in section 2.4 have been modelled with the model presented in sections 2.1, 2.2 and 2.3 implemented in the user subroutine UMAT of the software Abaqus. Material properties used in the numerical model (Tables 1 to 4) were defined in a cylindrical coordinate system, individually for each lamella, with the origin in its pith. In order to model the moisture transport, coupled temperature-displacement analyses were conducted in which the temperature variable was replaced by the MC. Therefore, the finite element type used in these analyses is the coupled temperature-displacement eight-node linear brick C3D8T. In the analyses, displacements of the bottom face of the specimens were prevented while all the other faces were free to move. A surface heat flux, representing the moisture flux, was applied to all

the vertical faces (refer to Figures 3 and 5). In the creep analyses, the top face of the specimens was loaded with constant pressure for the whole time period. In the relaxation analyses, a vertical displacement equivalent to an initial computed average stress of 1 and 0.8 MPa, respectively, was applied to the top face of the specimens. The vertical displacement of the top face of the specimens was afterwards fixed to represent the relaxation procedure.

3.2.1 RELAXATION ANALYSIS

The results from the specimen analyses in the relaxation tests show good overall agreement with the experimental results. The numerical results are directly compared to the experimental data in Figure 6.

The deviations of the numerical results compared to experiments are most prominent in periods with rapid humidity variations. A reason for such deviations can be the simplicity of the model (a single-Fickian approach) describing the moisture transfer. A more accurate modelling of moisture transfer might be based on a multi-Fickian approach that considers all the different phases of water in wood: water sorption in pores, bound water in cell walls and sorption between these two phases (Dvinskikh et al. 2011, Fortino et al. 2013). Nevertheless, the overall trend was followed and the differences between the numerical and the experimental results were small for the entire analysed period as depicted in Figure 6 where the term “stress” refers to the average compression stress. In Table 5, an assessment of the root mean square deviation (RMSD) of the model results with respect to the measured experimental values of the relaxation tests is provided.

Table 5: Root-mean-square deviation (RMSD) of the numerical results of the relaxation analyses at the end of the simulations (subscript end) and maximum (subscript max)

Specimen	Initial stress (MPa)	$RMSD_{end}$ (MPa)	$RMSD_{max}$ (MPa)
R-1.0	1.0	0.0662	0.0874
R-0.8	0.8	0.0882	0.0973

3.2.2 CREEP ANALYSIS

Results from the analyses of the nine specimens of creep tests are plotted in Figure 7. The difference in behaviour between the wetting and drying processes is confirmed as the use of a different shrinkage/swelling coefficient for the two phases properly describes the experimental results. Moreover, the numerical analyses depict different curves for each specimen although the compression stress is the same. This effect is solely due to the inclusion of the pith location of each lamella in the model. The pith location of each lamella is the only material variation used in the numerical models; otherwise, the material properties are identical for all the specimens as specified in Tables 1 to 4.

In Figure 7, the numerical simulations results are compared to the corresponding experimental measurements for each specimen and plotted separately for each stress level.

Similar to the numerical analyses of the relaxation tests, the accuracy is moderately lower in the case of quick humidity variation. However, the overall trend is well represented and the differences between the experimental and numerical strains are kept small for the whole time period. The long-term behaviour is well represented by the numerical analyses despite a higher deviation between numerical simulations and experimental data corresponding to the first humidity variation. This deviation might occur because the loading and moisture history of the material prior to the testing was not known. Moreover, the deviation increases in case of higher compression stress. Therefore, this could arguably suggest that the numerical model might have overestimated the irrecoverable mechanosorptive deformation of tested specimens. Additionally, the deviation might have occurred because of a non-accurate evaluation of the MC due to the simplicity of the single-phase moisture transport model.

All in all, the results for the two setups illustrate that the model described in sections 2.1, 2.2 and 2.3 behaves well with regard to the long-term behaviour of timber subjected to uniform perpendicular-to-grain compression under variable humidity conditions.

Table 6 provides an evaluation of the RMSD of the model results with respect to the measured experimental values of the creep tests.

Table 6: Root-mean-square deviation (RMSD) of the numerical results of the creep analyses at the end of the simulations (subscript end) and maximum (subscript max)

Specimen	Compression stress [MPa]	$RMSD_{end}$ [-]	$RMSD_{max}$ [-]
A-1.0	1.0	0.00144	0.00144
B-1.0	1.0	0.00280	0.00280
C-1.0	1.0	0.00085	0.00103
A-0.8	0.8	0.00083	0.00102
B-0.8	0.8	0.00093	0.00103
C-0.8	0.8	0.00089	0.00101
A-0.6	0.6	0.00097	0.00104
B-0.6	0.6	0.00090	0.00102
C-0.6	0.6	0.00102	0.00112

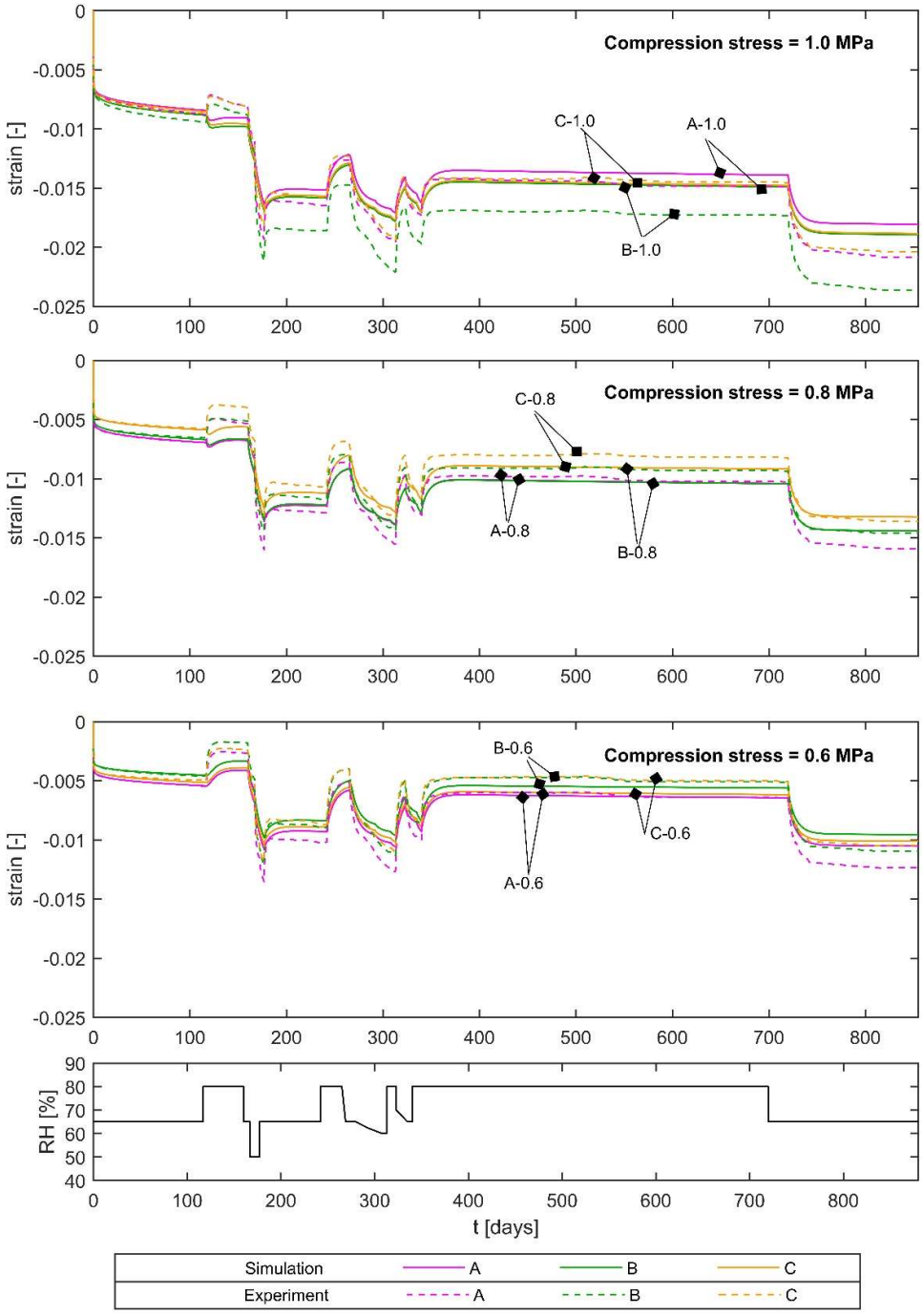

Figure 7: Comparison between numerical and experimental results of the creep tests and relative humidity (RH) of the air during the creep tests (Norway spruce).

4. CONCLUSION

The objective of this study was to validate a numerical model describing the long-term behaviour of Norway spruce in the perpendicular-to-grain direction and calibrate the necessary model parameters for proper three-dimensional (3D) description of the deformations in this direction.

The model considers elastic strain, hygroscopic strain, viscoelastic strain and mechanosorptive strain. The viscoelastic strain is distributed in six Kelvin bodies. The mechanosorptive strain is distributed in three Kelvin bodies. The asymptotic property of Kelvin bodies allows the realisation of a physically acceptable solution requiring a few parameters to fit. An additional mechanosorptive dashpot accounts for the irrecoverable part of the mechanosorptive strain.

The examination of the results from the relaxation experiments performed under constant RH confirmed the non-linear dependency of the strain with respect to the stress (Figure 6), observed also in experimental creep tests. This effect is considered in the numerical model by introducing a non-linear equation for evaluating the viscoelastic parameters.

The numerical model considers the pith locations of each lamella, as previous studies have demonstrated their significance and their influence in the evaluation of the wood deformation. Other possible variations of material properties have been excluded from this study.

The numerical model allows a proper description of the creep and relaxation phenomena occurring in Norway spruce under compression perpendicular to the grain. The 3D approach displayed an overall good agreement between the experimental and numerical results. The RMSD of the model is in the order of 10% of the maximum stress/strain which yields acceptable results for the study of stress-laminated bridge decks. However, the deviations can possibly be further reduced by investigations carrying out more sophisticated material characterisations of the test specimens in the different material directions. Moreover, improving the moisture

transfer model using a multiphase approach might reduce the deviations, especially with respect to sudden RH changes.

ACKNOWLEDGMENTS

This work was funded by the WoodWisdom-Net+ project DuraTB ("Durable Timber Bridges") and the support from the funding bodies and partners is gratefully acknowledged.

REFERENCES

Angst, V., Malo, K.A. (2012) The effect of climate variations on glulam—an experimental study. Eur. J. Wood Wood Prod. 70:603-613.

Angst, V., Malo, K.A. (2013) Moisture-induced stresses in glulam cross sections during wetting exposures. Wood Sci. Technol. 47:227-241.

Avramidis, S. (1989) Evaluation of "three-variable" models for the prediction of equilibrium moisture content in wood. Wood Sci. Technol. 23:251-257.

CEN (2016) Structural timber - Strength classes. EN 338:2016.

CEN (2013) Timber structures - Glued laminated timber and glued solid timber. EN 14080:2013.

Dahl, K.B. (2009) Mechanical properties of clear wood from Norway spruce. Norwegian University of Science and Technology, Trondheim.

Dahl, K.B., Malo, K.A. (2009) Linear shear properties of spruce softwood. Wood Sci. Technol. 43:499-525.

Dassault Systemes (2014) Abaqus/CAE 6.14.

Dinwoodie, J.M. (2000) Timber: Its Nature and Behaviour. E & FN Spon - Taylor & Francis, London & New York.

Dvinskikh, S.V., Henriksson, M., Mendicino, A.L., Fortino, S., Toratti, T. (2011) NMR imaging study and multi-Fickian numerical simulation of moisture transfer in Norway spruce samples. Eng. Struct. 33:3079-3086.

Fortino, S., Genoese, A., Genoese, A., Nunes, L., Palma, P. (2013) Numerical modelling of the hygro-thermal response of timber bridges during their service life: A monitoring case-study. Constr. Build. Mater. 47:1225-1234.

Fortino, S., Mirianon, F., Toratti, T. (2009) A 3D moisture-stress FEM analysis for time dependent problems in timber structures. Mech. Time-Depend. Mater. 13:333-356.

Hanhijärvi, A. (1995) Modelling of creep deformation mechanisms in wood. Technical Research Centre of Finland VTT, Espoo.

Hanhijärvi, A., Mackenzie-Helnwein, P. (2003) Computational Analysis of Quality Reduction during Drying of Lumber due to Irrecoverable Deformation. I: Orthotropic Viscoelastic-Mechanosorptive-Plastic Material Model for the Transverse Plane of Wood. J. Eng. Mech. 129:996-1005.

Hunt, D.G. (1994) Present knowledge of mechano-sorptive creep of wood. In: RILEM Report 8 - Creep in Timber Structures. Morlier, P. E & FN Spon, London. pp. 73-97.

Lagaňa, R., Davids, W.G., Muszyński, L., Shaler, S.M. (2011) Moment-curvature analyis of coupled bending and mechanosorptive response of red spruce beams. Wood and Fiber Science. 43:280-292.

Morlier, P., Palka, L.C. (1994) Basic knowledge. In: RILEM Report 8 - Creep in Timber Structures. Morlier, P. E & FN Spon, London. pp. 9-42.

Muszyński, L., Lagaňa, R., Shaler, S.M., Davids, W.G. (2005) Comments on the experimental methodology for determination of the hygro-mechanical properties of wood. Holzforschung. 59:232-239.

Ozyhar, T., Hering, S., Niemz, P. (2013) Viscoelastic characterization of wood: Time dependence of the orthotropic compliance in tension and compression. Journal of Rheology. 57:699-717.

Salin, J.-G. (1992) Numerical prediction of checking during timber drying and a new mechano-sorptive creep model. Holz als Roh- und Werkstoff. 50:195-200.

Santaoja, K., Leino, T., Ranta-Maunus, A., Hanhijärvi, A. (1991) Mechano-sorptive Structural Analysis of Wood by the ABAQUS Finite Element Program. VTT, Espoo.

Schniewind, A.P. (1968) Recent progress in the study of the rheology of wood. Wood Sci. Technol. 2:188-206.
Sjödin, J. (2006) Steel-to-timber dowel joints: Influence of moisture induced stresses. Vaxjo University, Vaxjo.
Svensson, S., Toratti, T. (2002) Mechanical response of wood perpendicular to grain when subjected to changes of humidity. Wood Sci. Technol. 36:145-156.
Toratti, T. (1992) Creep of timber beams in a variable environment. Helsinki University of Technology, Espoo.
Zienkiewicz, O.C., Watson, M., King, I.P. (1968) A numerical method of visco-elastic stress analysis. Int. J. Mech. Sci. 10:807-827.